Brigham Young University
BYU ScholarsArchive

Faculty Publications

2023-03-07

Membrane-enhanced Lamina Emergent Torsional Joints for Surrogate Folds

Guimin Chen
Xi'an Jiaotong University

Spencer P. Magleby
Brigham Young University - Provo, magleby@byu.edu

Larry L. Howell
Brigham Young University - Provo, lhowell@byu.edu

Follow this and additional works at: https://scholarsarchive.byu.edu/facpub

 Part of the Mechanical Engineering Commons

Original Publication Citation

Chen, G., Magleby, S.P., and Howell, L.L., "Membrane-enhanced Lamina Emergent Torsional Joints for Surrogate Folds," Journal of Mechanical Design, Vol. 140, 062303-1 to 062303-10, DOI: 10.1115/1.4039852, 2018.

BYU ScholarsArchive Citation

Chen, Guimin; Magleby, Spencer P.; and Howell, Larry L., "Membrane-enhanced Lamina Emergent Torsional Joints for Surrogate Folds" (2023). *Faculty Publications*. 6586.
https://scholarsarchive.byu.edu/facpub/6586

This Peer-Reviewed Article is brought to you for free and open access by BYU ScholarsArchive. It has been accepted for inclusion in Faculty Publications by an authorized administrator of BYU ScholarsArchive. For more information, please contact ellen_amatangelo@byu.edu.

Membrane-enhanced Lamina Emergent Torsional Joints for Surrogate Folds

Guimin Chen[1,2], Spencer P. Magleby[2] and Larry L. Howell[2]

[1] State Key Laboratory for Manufacturing Systems Engineering, Xi'an Jiaotong University, 710049 Xi'an, China

[2] Department of Mechanical Engineering, Brigham Young University, Provo, UT 84602, USA

Abstract

Lamina emergent compliant mechanisms (including origami-adapted compliant mechanisms) are me chanical devices that can be fabricated from a planar material (a lamina) and have motion that emerges out of the fabrication plane. Lamina emergent compliant mechanisms often exhibit undesirable para sitic motions due to the planar fabrication constraint. This work introduces a type of lamina emergent torsion (LET) joint that reduces parasitic motions of lamina emergent mechanisms (LEMs), and presents equations for modeling parasitic motion of LET joints. The membrane joint also makes possible one-way joints that can ensure origami-based mechanisms emerge from their flat state (a change point) into the desired configuration. Membrane enhanced LET joints, including one-way surrogate folds, are described here and show promise for use in a wide range of compliant mechanisms and origami-based compliant mechanisms. They are demonstrated as individual joints and in mechanisms such as a kaleidocycle (a 6R Bricard linkage), degree-4 origami vertices (spherical mechanisms), and waterbomb base mechanisms (an 8R multi-degree-of-freedom origami-based mechanism).

1 Introduction

Lamina emergent torsional (LET) joints [1] were devised to facilitate the design of compliant mechanisms that can be fabricated from a planar material but have motion that emerges out of the fabrication plane as shown in Figure 1 [2]. A LET joint consists of two parallel sets of torsional segments connected by relatively stiff connecting segments. When the torsional segments are on the outside of the joint, it is called an outside LET joint (see Figure 2), and if they are on the inside of the joint, it is called an inside LET joint (see Figure 3). A LET joint primarily provides one rotational degree-of-freedom through the torsional deflections of the 1

torsional segments, as illustrated in Figures 2 and 3.

LET joints have been employed as surrogate folds for creases in origami-based engineering designs [3]. An outside LET joint was used for high precision positioning in the national ignition facility target

shroud s [4]. A few variations (outside-deployed LET joints and triple-LET joints) of LET joints were devised to increase the angular displacement range of LET joints [5, 6].

An ideal replacement for a traditional revolute joint, or an ideal surrogate fold, would allow unre strained rotation about the joint axis (*x*-axis in Figures 2 and 3) but have infinite stiffness in all other directions. Therefore, LET joints would have low torsional stiffness while maintaining high stiffness in the other directions [1]. However, they are susceptible to undesired motion when a compressive/tensile load or an in-plane moment is applied because the torsional segments are placed into bending, as illustrated in Figures 4 and 5. Therefore, they are not suitable for high precision applications if these types of loads are applied. Rotations other than the rotation about the desired axis of rotation are considered parasitic motions. The parasitic motions that tend to be largest and most problematic are rotation about the z-axis and translation in the y direction and they receive the most attention in this work.

Figure 1: A lamina emergent four-bar mechanism that utilizes LET joints as its revolute pairs [1].

Research has been done to reduce these parasitic motions [7] and some design insights for LET joints have been provided in [8], but the improvement is limited. Membranes were utilized as surrogate folds to reduce in-plane parasitic motion, for example, Zirbel et al. [9] connected rigid and thick panels using a flexible membrane with gap spacing to accommodate the thickness so as to enable rigid foldability, and Ku et al. [10] employed a membrane to act as living hinges between adjacent panels for folding thick materials. If a membrane joint is made with sufficient rigidity to withstand off-axis motions and buckling, then its stiffness also increases about the axis of desired motion.

This work introduces a way to reduce the parasitic motions of both outside and inside LET joints by 2

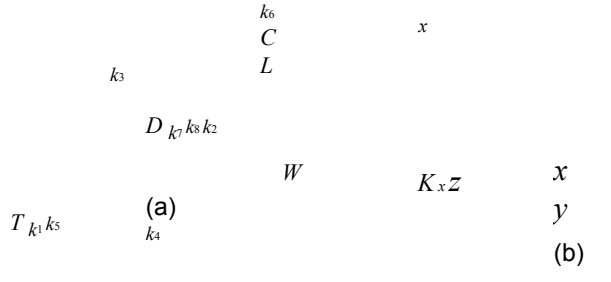

Figure 2: (a) An outside LET and (b) its intended deflection.

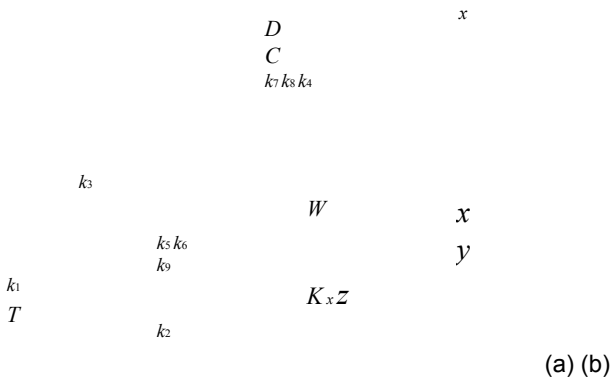

Figure 3: (a) An inside LET and (b) its intended deflection.

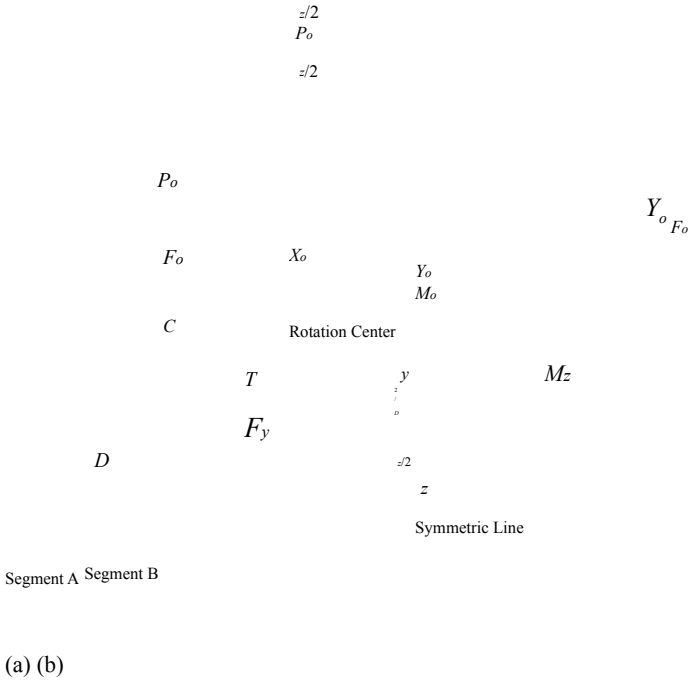

Figure 4: In-plane parasitic motion of an outside LET joint, including (a) tensile deflection (translation along the *y*-axis) and (b) in-plane rotational deflection (rotation around the *z*-axis).

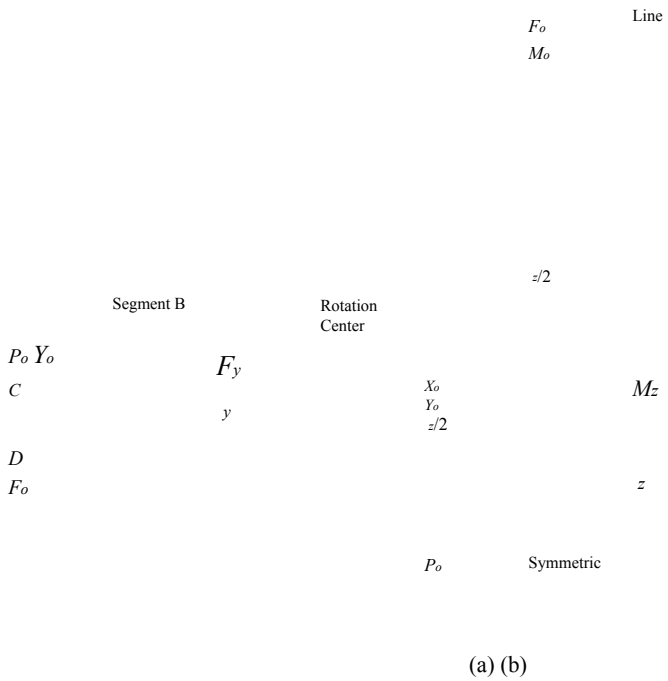

Figure 5: In-plane parasitic motion of an inside LET joint, including (a) tensile deflection (translation along the *y*-axis) and (b) in-plane rotational deflection (rotation around the *z*-axis).

integrating a membrane, leading to a class of LET joints called membrane-enhanced LET joints (M-LET joints). The membrane changes the inherent characteristics of the LET joint, and those changes can be exploited to achieve desired effects, such as reducing parasitic motion and creating one-way surrogate folds.

Models describing the parasitic motions of LET joints are developed next, followed by the introduction of membrane-enhanced joints. The M-LET combines advantages of LET joints and membrane flexures (e.g. large angular displacements) and mitigates some of their individual disadvantages (e.g. parasitic motions and low buckling resistance), but at the cost of assembling a composite joint. Unidirectional M-LET joints are introduced in the paper and they help constrain motion to guide mechanisms through change points and to provide desired motions. M-LET joints will be useful for creating lamina emergent mechanisms, and show particular promise for origami-based mechanisms. M-LET joints are demonstrated in several different mechanisms throughout the paper.

2 Modeling Parasitic Motions of LET Joints

To evaluate the need of the membrane-enhanced LET joint and to develop the new joints, it is important to understand the parasitic motions associated with LET joints. Preliminary modeling of LET joints has been done in previous work [1, 3]. The spatial deflection of LET joints can be modeled using the methods developed in Refs. [17–20]. Ideally, a LET joint would have motion similar to a hinge with infinite stiffness

in other directions. Models to describe their flexibility in off-axis directions are developed in this section.

2.1 Tensile/compressive Stiffness

When a LET joint is subject to a tensile/compressive load F_y (yielding a deflection Δ_y), each of the torsional segments can be treated as fixed-guided segments [21]. We denote the transverse force, the axial force and the moment applied on each segment as F_o, P_o and M_o, and the corresponding transverse and axial deflections as Y_o and X_o, respectively, as illustrated in Figure 4(a) and Figure 5(a).

For an outside LET joint, because the axial force applied on each torsional segment $P_o = 0$, utilizing the closed-form solution of Bi-BCM [24] yields

$$f_o = 3y_o \quad (1)$$

where y_o and f_o are the transverse deflection and the transverse force normalized with respect to $L/2$, given as:

$$L = \Delta_y \qquad 4EI = F_y L^2$$
$$y_o = 2Y_o$$
$$L,\ f_o = F_o L^2 \qquad 8EI \quad (2)$$

in which L, W, T and I are the length, the in-plane thickness, the out-of-plane thickness and the area moment of inertia of the torsional segment ($I = WT^3/12$), respectively, and E is the elastic modulus of the material. Then the tensile/compressive stiffness can be expressed as:

$$F_y$$
$$\Delta_y = 12EI \quad (3)$$
$$L^3$$

For an inside LET joint, the axial displacement of each torsional segment is $X_o = 0$. Utilizing the closed-form solution of Bi-BCM [24] yields the normalized axial force p_o and the normalized transverse force f_o expressed as a function of y_o:

$$+ 720$$
$$p_o = B_3 - A_2$$
$$A_1 B_3,\ f_o = 9p^2{}_o + 312p_o$$
$$A_1 - B_1$$
$$16p_o + 480\ y_o \quad (4)$$

where

$14000,\ A_2 = 16t^2$

$2100,\ A_3 = 16t^2$

$A_1 = 4t^2$

$225y_o^2 + 1 \quad 3y_o^2 - 96 \quad (\quad)^{1/3}$

$45y_o^2 - 17 \quad 175, \quad \sqrt{}$

$B_1 = A_1A_3 - A^2{}_2,\ B_2 = A^3{}_2,\ B_3 = B^3{}_1 + B^2{}_2$

$1.5A_1(A_2A_3 + 9.6A_1) - B_2 +$

in which $t = 2T/L$. Then the tensile/compressive stiffness can be expressed as: F_y

$$\Delta_y = 9p_o^2 + 312p_o + 720\ 2p_o + 60 \quad \frac{EI}{L^3} \quad (5)$$

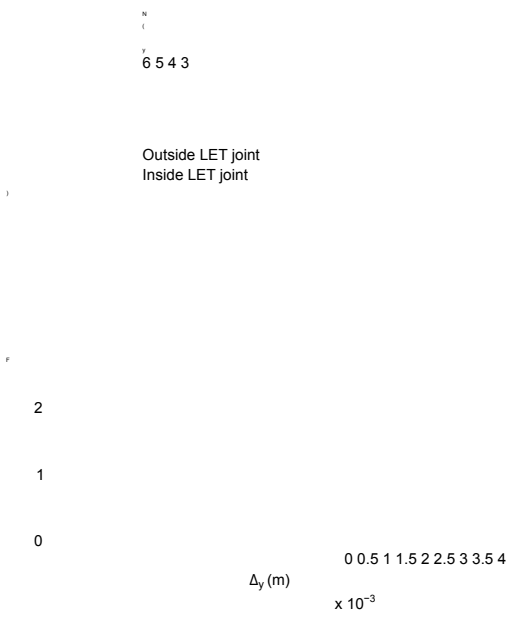

Figure 6: Tensile/Compressive stiffness comparison of outside and inside LET joints. Joint parameters: L = 30 mm, W = 1.5 mm, T = 1.5 mm and $E = 1.4 \times 10^9$ Pa.

Figure 6 compares the curves of F_y vs. Δ_y of an outside LET joint and an inside LET joint with identical torsional segments. It shows that the inside and the outside LET joints exhibit the same stiffness at the as-fabricated position, however, the inside LET joint becomes stiffer when deflected due to stress stiffening of the torsional segments.

2.2 In-plane Rotational Stiffness

When a LET joint is subject to an in-plane moment, the torsional segments can be modeled as illustrated

in Figure 4(b) and Figure 5(b).

For the outside LET joint: we assume that the outside LET joint yields an in-plane rotation of θ_z due to the applied moment M_z. Considering the symmetry of the joint (note that the symmetric line rotates around the rotation center), the end slope of each torsional segment $\theta_o = \theta_z/2$, and we have the following load relations:

$$\begin{aligned} &P_o \cos\theta_o + F_o \sin\theta_o = 0 \\ &2[F_o(L + X_o + 0.5D) - P_oY_o + M_o] = M_z \end{aligned} \quad (6)$$

and the following deflection relation:

$$\frac{Y_o - 0.5C + 0.5C\cos\theta_o}{L + X_o + 0.5D - 0.5C\sin\theta_o} = \tan\theta_o \quad (7)$$

where C is the length of the middle connecting segment along the x-axis (k_6), D is the length of the side connecting segment (k_7). The transverse force and the axial force at the torsional segment are denoted as F_o and P_o, respectively. The beam constraint model (BCM) [25] formulates the load-deflection relations of the segment as:

$$\begin{bmatrix} \frac{F_oL^2}{EI} \\ \frac{M_oL}{EI} \end{bmatrix} = \begin{bmatrix} 12 & -6 \\ -6 & 4 \end{bmatrix} \begin{bmatrix} \frac{Y_o}{L} \\ \theta_o \end{bmatrix} + \frac{P_oL^2}{EI} \begin{bmatrix} 6/5 & -1/10 \\ -1/10 & 2/15 \end{bmatrix} \begin{bmatrix} \frac{Y_o}{L} \\ \theta_o \end{bmatrix} + \left(\frac{P_oL^2}{EI}\right)^2 \begin{bmatrix} -1/700 & 1/1400 \\ 1/1400 & -11/6300 \end{bmatrix} \begin{bmatrix} \frac{Y_o}{L} \\ \theta_o \end{bmatrix} \quad (8)$$

and

$$\frac{X_o}{L} = \frac{P_oT^2}{12EI} - \frac{1}{2}\begin{bmatrix} \frac{Y_o}{L} & \theta_o \end{bmatrix} \begin{bmatrix} 6/5 & -1/10 \\ -1/10 & 2/15 \end{bmatrix} \begin{bmatrix} \frac{Y_o}{L} \\ \theta_o \end{bmatrix} - \frac{P_oL^2}{EI} \begin{bmatrix} \frac{Y_o}{L} & \theta_o \end{bmatrix} \begin{bmatrix} -1/700 & 1/1400 \\ 1/1400 & -11/6300 \end{bmatrix} \begin{bmatrix} \frac{Y_o}{L} \\ \theta_o \end{bmatrix} \quad (9)$$

For the inside LET joint: we assume that the inside LET joint produces an in-plane rotation of θ_z due to the applied moment M_z. The rotation center of the middle connecting segment is assumed to be located at the center of its left side (as shown in Figure 5(b)) because this leads to least energy stored in the joint. The corresponding tip deflections of each torsional segment are:

$$\begin{aligned} &\theta_o = \frac{\theta_z}{2} \\ &X_o = 0.5D(1 - \cos\theta_o) \\ &Y_o = -0.5D\sin\theta_o \end{aligned} \quad (10)$$

where D is the length of the middle connecting segment along the x-axis. The transverse force and the axial force at the torsional segment are denoted as F_o and P_o, respectively. BCM [25] formulates the load-deflection relations of the segment as:

$$\begin{bmatrix} F_o L^2 / EI \\ M_o L / EI \end{bmatrix} = \begin{bmatrix} 12 & -6 \\ -6 & 4 \end{bmatrix} \begin{bmatrix} Y_o / L \\ \theta_o \end{bmatrix} + P_o L^2 / EI \begin{bmatrix} 6/5 & -1/10 \\ -1/10 & 2/15 \end{bmatrix} \begin{bmatrix} Y_o / L \\ \theta_o \end{bmatrix} \quad (11)$$

and

$$L = P_o T^2 / 12EI \left[-\frac{1}{2} \begin{bmatrix} Y_o \\ \theta_o L \end{bmatrix} + \begin{bmatrix} 6/5 & -1/10 \\ -1/10 & 2/15 \end{bmatrix} \begin{bmatrix} Y_o \\ \theta_o L \end{bmatrix} - P_o L^2 / EI \begin{bmatrix} -1/70 & 0 \\ 0 & 1/1400 \end{bmatrix} \begin{bmatrix} Y_o \\ \theta_o L \end{bmatrix} \right] \quad (12)$$

For a given θ_z, Eq. (12) is used to solve for P_o, which can be substituted into Eq. (11) for F_o and M_o. Then M_z can be obtained as:

$$M_z = 2 \left(M_o - F_o D \right) \cos \theta_o + P_o D \sin \theta_o \quad (13)$$

Figure 7 plots the curves of M_z vs. θ_z of an outside LET joint and an inside LET joint with identical torsional segments. It shows that the inside and the outside LET joints exhibit the same stiffness at the as-fabricated position, however, the inside LET joint becomes slightly stiffer when deflected due to stress stiffening of the torsional segments.

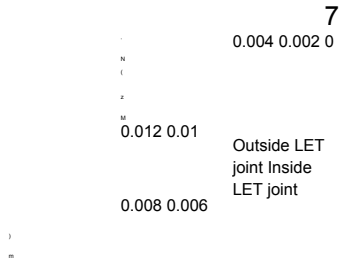

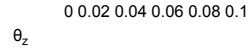

Figure 7: In-plane rotational stiffness comparison of inside and outside LET joints. The parameters of the joints are: L = 30 mm, T = 1.5 mm, W = 1.5 mm, C = 2 mm, D = 5 mm and $E = 1.4 \times 10^9$ Pa.

3 Membrane-enhanced LET Joints

A very thin and flexible sheet (e.g., a fabric) has properties similar to blade flexures but alone may be too flexible to act as flexures [9]. However, a membrane has stiffness in directions where LET joints have undesired flexibility. Combining a membrane with a LET joint has the potential of creating a joint with desired flexibility with minimal parasitic motions (high off-axis stiffness). Besides, the compressive stiffness of LET joints can reduce the risk of membrane bucking.

Figure 8 lists some configurations of membrane-enhanced LET (M-LET) joints by combining membranes with LET joints. The membranes constrain motion in undesired directions while not inhibiting the motion in the desired direction of LET joints. The membrane and the LET joints can be fully bonded such that the torsional segments are attached the membrane, or partially bonded such that the torsional segments and the membrane are separate. Generally speaking, fully bonded designs have larger stiffnesses in the desired direction of motion than partially bonded ones due to the coupling between the bending deflections of the membrane and the torsional deflections of the torsional segments. Because of the twisting motion in the torsion beams, there is a greater chance of delamination in fully bonded LET joints. Whether delamination occurs depends on the structure (sandwich versus bilayer), the induced stresses (which depend on geometry, magnitude of deflection, and material properties), and how the layers are adhered. If delamination occurs in a fully bonded joint, then it may become a partially bonded M-LET.

Figure 9 shows a prototype of a sandwich M-LET joint at its undeflected and deflected positions. The

Inside LET Outside LET
Fully Bonded Partially Bonded Fully Bonded Partially Bonded

designs.

Figure 8: Various M-LET joint

membrane is placed in between two LET joints. Figure 10 shows a prototype of a bilayer M-LET joint at its undeflected and deflected positions. The membrane is attached to one side of the LET joint. In these examples, the LET joint is made of polypropylene and the membrane from metallic glass [26]. The boundary conditions for the fully bonded design are complicated and numerical models are recommended for their detailed analysis.

3.1 Membrane Addition

A thin sheet of material (also called a sheet flexure or blade flexure in compliant mechanisms), as illustrated in Figure 11, can provide ideal constraints for the parasitic motions of LET joints (the displacement along the *y*-axis and the rotation about the *z*-axis) while maintaining the rotation about the *x*-axis [11, 12].

The addition of the membrane slightly increases the stiffness of the joint in the desired direction of motion. The bending stiffness of the membrane can be expressed as:

$$\alpha_x = \frac{E' I_x}{L_s} \qquad K_{\alpha x} = M_x \tag{14}$$

where I_x is the area moment of inertia

$$I_x = \frac{T_s W^3}{}$$

12 (15) 9

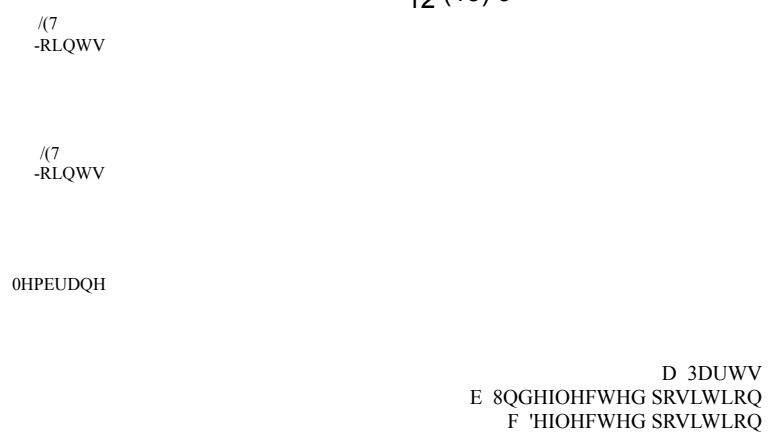

Figure 9: A sandwich membrane-enhanced outside LET joint. The LETs are made of polypropylene and the membrane from metallic glass.

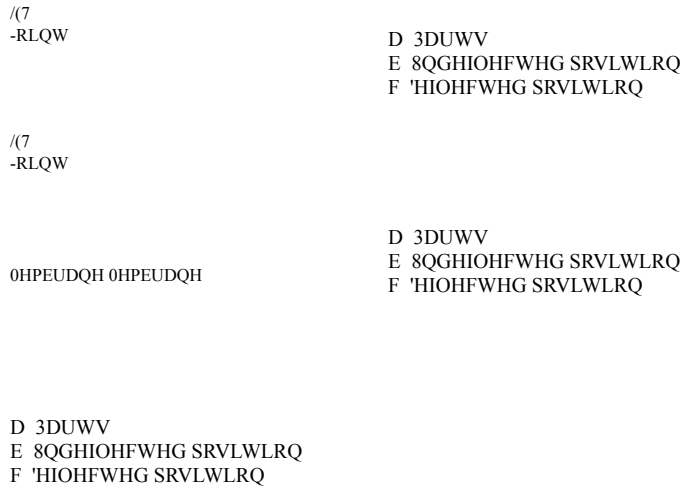

Figure 10: A bilayer membrane-enhanced outside LET joint. The LET is made of polypropylene and the membrane from metallic glass.

and $E_s^{'}$is the plate modulus given as [40]

$$E_s^{'} = \frac{E_s}{1 - v_s^2} \quad (16)$$

in which E_s, v_s, L_s, T_s are W_s are the Young's modulus, the Poisson's ratio, the effective length, the width and the thickness of the membrane, respectively. However, membrane significantly increases the ten sile/compressive stiffness and the in-plane rotational stiffness (plane stress is assumed [40]):

$$K_{\Delta y} = \frac{F_y}{\Delta_y} = \frac{E_s A_s}{L_s} \quad (17)$$

where $A_s = w_s t_s$, and

$$K_{\alpha z} = \frac{M_z}{\alpha_z} = \frac{E_s I_z}{L_s} \quad (18)$$

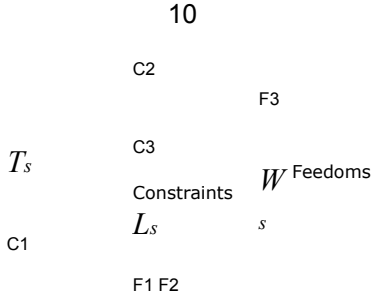

Figure 11: Constraint space and freedom space of a sheet flexure.

Table 1: Parameters of LET joint and membrane.

Parameter	E/E_s	G	v_s	T/T_s	W/W_s	L/L_s	C	D
LET joint (polypropylene)	1.4 × 10⁹ Pa		5.2 × 10⁸ Pa	-	1.5 mm	1.5 mm	10 mm	2 mm	3 mm
Membrane (metallic glass)	9.5 × 10¹⁰ Pa		-	0.3	27 mm	0.1 mm	6 mm	-	-

where $I_z = W_s T_s^3/12$. It should be noted the above stiffness expressions are valid when the loads don't exceed the critical buckling loads.

There is a significant distinction between a membrane in tension and in compression because they are stiff in tension but tend to buckle in compression. The M-LET does not count on the membrane for significant resistance to compressive forces. However, in the sandwich M-LET, the membrane is constrained between two LET layers, which provides considerable buckling resistance. Because the unsupported membrane lengths are small in a fully bonded M-LET, buckling also constrained. In a later section it will be shown that the difference between tension and compression can be exploited to create unidirectional joints, and that additional structures can be included to provide buckling resistance.

3.2 Membrane Impact on Stiffness

Consider an M-LET joint (bilayer structure and partially bonded) whose parameters are listed in Table 1 and configured as an outside LET joint with parameters described in Figures 2 and 11. The LET joint is made of polypropylene and the membrane from metallic glass. The stiffnesses of the LET joint and the membrane are compared in Table 2, in which the torsional stiffness of the LET joint ($K_{\alpha x}$) is calculated using the symmetric equation obtained in Ref. [23] as

$$K_t = \frac{G}{L}\cdot\frac{7(T^2 + W^2)\cdot 1.17\frac{T}{2}}{2T^3W^3\left(\frac{W}{2}\right)^2 + 2.191\frac{T}{2}\left(\frac{W}{2}\right) + 1.17}$$

$$\left(\frac{W}{2}\right)^2 + 2.609\frac{T}{2}\left(\frac{W}{2}\right) + 1(19)\left(\frac{T}{2}\right)^2$$

The comparison shows that the inclusion of the membrane increases the stiffnesses of the translation along the *y*-axis and the rotation around the *z*-axis by more than five thousand times, while only increasing the rotation stiffness around the *x*-axis about one time.

Table 2: Stiffness comparison of LET joint and membrane.

Stiffness	$K_{\alpha x}$	$K_{\Delta y}$	$K_{\alpha z}$
LET joint	0.037 N· m	7088 N/m	0.3685 N· m
Membrane	0.039 N· m	4.275×10^7 N/m	2597 N· m

Stop Blocks

Membrane

(a) (b)

Figure 12: Realization of unidirectional foldability of M-LET joints (bilayer structure) by adding stop blocks (with the gaps exaggerated) combined with a bilayer structure.

3.3 Unidirectional Surrogate Folds

The bilayer structure makes it possible to create a unidirectional surrogate fold. For most origami-inspired designs, it is desirable to use unidirectionally rotatable joints for surrogate folds to ensure mountain and valley fold parity. Because origami-based mechanisms are often fabricated in the planar state, the as fabricated position represents a change-point where joints could fold either up or down into either a mountain or a valley fold, so a joint architecture that defines the fold direction can be valuable. Figure 12(a) shows a modified membrane-enhanced outside LET joint in which a stop block is employed and the membrane is glued on the back side for the purpose of preventing the adjacent facets from folding up out of the flat plane at the fold (mountain fold). Similarly, Figure 12(b) shows a modified membrane-enhanced inside LET joint in which two stop blocks are added to prevent the adjacent facets from folding up out of

the flat plane. The stop blocks also help to eliminate the risk of buckling of the membranes.

4 Examples

This section compares LET joints and membrane-enhanced LET joints in several compliant mechanism de signs. Because they show great promise for use as surrogate folds in origami-based compliant mechanisms, origami-inspired examples are emphasized.

3DUDVLWLF DQJOH

Figure 13: Kaleidocycle with joints replaced by outside LET joints fabricated in acrylic.

4.1 Kaleidocycles with LET and M-LET Joints

Kaleidocycles are *n*-jointed linkages that allows infinite rotation [28]. Figure 13 shows a fully compliant six-jointed kaleidocycle utilizing LET joints as its joints. The pseudo-rigid-body model [21] of the device is a Bricard 6R mechanism [35, 36] and can be modeled using spatial mechanism approaches [37–39]. From Figure 13 we can see large parasitic in-plane rotation of the LET joints and the contacts between torsional segments. An ideal joint would only have motion about the desired axis of rotation, but Figure 13 shows the parasitic rotation of a kaleidocycle LET joint with undesired rotation about the joint's *z*-axis (the angle labeled in the figure would be equal to zero if there were no parasitic motion). Figure 14 shows a kaleidocycle with the joints replaced by M-LET joints (sandwich structure and partially bonded) at different positions.

The parasitic deflections have been well constrained (i.e. there is negligible rotation about the *z*-axis for individual M-LET joints), and no contact between torsional segments is detected.

4.2 Thick Degree-4 Vertex with Bilayer M-LET Joints

Figure 15 shows an origami-adapted compliant mechanism design based on a degree-4 vertex. The degree 4 vertex is rigidly foldable, which means that it can be folded without deforming the panels. The sector angles of the four panels are 120°, 90°, 90° and 60°, respectively. Membrane-enhanced LET joints of bilayer structure and fully bonded are employed in the design. Having the membrane on different sides of the structure results in an offset of the joint axes by the thickness of the panel material. Figure 16 shows the

design at different folding positions, including the fully folded position in Figure 16(c). The utilization of membrane-enhanced LET joints helps reducing parasitic motions and increasing precision and repeatability of the design.

Figure 17 shows a different design of the degree-4 vertex employing unidirectional M-LET joints. For

Figure 14: Kaleidocycles employing membrane-enhanced LET joints. The LET joint is made of polypropy lene and the membranes are from metallic glass.

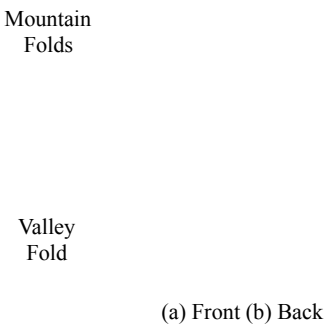

(a) Front (b) Back

Figure 15: Thick degree-4 vertex using bilayer structure M-LET joints.

the mountain folds (where the adjacent facets point up out of the flat plane at the folds), the membrane is attached on the back, while for the valley fold (where the adjacent facets point down where they meet), the membrane is on the front. Figure 18 shows the design at different folding positions. The utilization of the unidirectional M-LET joints enforces mountain and valley parity and makes it easy to fold.

4.3 Waterbomb Origami with Bilayer M-LET Joints

An origami waterbomb base is a single-vertex origami pattern having four mountain folds alternating with four valley folds around the vertex [30–34]. It is also rigidly foldable. Compliant surrogate hinges can be implemented in thick, rigid materials to mimic bending with minimal parasitic motion [27].

Figures 19 and 21 show thick waterbomb bases at their undeflected position. The designs utilizes unidi rectionally foldable M-LET joints (bilayer structure) for surrogate mountain/valley folds. The unidirectional foldable M-LET joints (as surrogate folds) enable us to predetermine the mountain and valley folds and

Figure 16: Different folding positions of the thick degree-4 vertex.

Figure 17: Thick degree-4 vertex using a bilayer structure that enforces mountain and valley parity.

benefit the folding process. Figures 20 and 22 show the waterbomb bases at different folded positions.

5 Conclusions

This paper introduces membrane-enhanced lamina emergent torsional (M-LET) joints. The membrane adds a minimal increase in stiffness in the desired direction of motion, but it significantly increases stiffness in directions that the traditional LET joint have undesired parasitic motion. The integration of M-LET joints as surrogate folds can reduce parasitic motions and increase precision and repeatability. The membrane enhanced arrangement enables the introduction of features that result in unidirectional motion, which is particularly helpful in guiding the motion of origami-based mechanisms out of their initial flat state

(a) (b)

(c) (d)

Figure 18: Different folding positions of the thick degree-4 vertex.

(which is also a change point) into the desired configuration. While the introduction, description, and demonstration of these concepts are the primary contributions of the paper, the equations derived here to model the parasitic motion of LET joints are valuable for predicting behavior of LET joints in general. They may also be helpful for evaluating if the anticipated parasitic motions of a LET joint justify the small increased cost of adding a membrane for an M-LET.

6 Acknowledgment

The authors gratefully acknowledge the financial support from the National Science Foundation Research of the United States under Grant No. 1663345, the National Natural Science Foundation of China under Grant No. 51675396, and the Fundamental Research Funds for the Central Universities under No. K5051204021.

Mountain Folds

Valley Fold

0RXQWDLQ)ROGV

9DOOH\
)ROG

Figure 19: A thick waterbomb base at its undeflected position. Unidirectionally foldable membrane enhanced LET joints (bilayer structure) for surrogate mountain/valley folds (the membrane is attached on the back for each mountain fold, while the membrane is attached on the front for each valley fold). A red membrane is used for mountain folds and a transparent membrane for valley folds.

Figure 20: The thick waterbomb base at different folded positions. The LETs are made of acrylic and the membranes from polyvinyl chloride.

References

[1] Jacobsen, J. O., Chen, G., Howell, L. L. and Magleby, S. P., 2009, “Lamina emergent torsion (LET) joint,” *Mechanism and Machine Theory*, vol. 44, no. 11, 2098-2109.

[2] Nelson, T. G., Lang, R. L., Pehrson, N., Magleby, S. P., Howell, L. L., 2016, “Facilitating Deployable Mechanisms and Structures via Developable Lamina Emergent Arrays,” *ASME Journal of Mechanisms and Robotics*, 8, 031006.

[3] Delimont, I.L., Magleby, S.P., Howell, L.L., 2015, “Evaluating Compliant Hinge Geometries for Origami Inspired Mechanisms,” *ASME Journal of Mechanisms and Robotics*, 7, 1, 011009.

[4] Boehm, K.J., Gibson, C.R., Hollaway, J.R. and Espinosa-Loza, F., 2016, “A Flexure-Based Mechanism for Precision Adjustment of National Ignition Facility Target Shrouds in Three Rotational Degrees of Freedom,” *Fusion Science and Technology*, 70(2), 265-273.

Figure 21: A thick waterbomb base at its undeflected position. Unidirectionally foldable membrane enhanced LET joints (bilayer structure) for surrogate mountain/valley folds (the membrane is attached on the back for each mountain fold, while the membrane is attached on the front for each valley fold).

(a) (b)

Figure 22: The thick waterbomb base at different folded positions. It is made of polypropylene and a composite tape for the membrane.

[5] Xie, Z., Qiu, L. and Yang, D., 2017, “Design and analysis of Outside-Deployed Lamina Emergent Joint (OD-LEJ),” *Mechanism and Machine Theory*, 114, pp.111-124.

[6] Qiu, L., Yin, S. and Xie, T., 2016, “Failure analysis and performance comparison of Triple-LET and LET flexure hinges,” *Engineering Failure Analysis*, 66, 35-43.

[7] Wilding, S.E., Howell, L.L., Magleby, S.P., 2012, “Introduction of Planar Compliant Joints Designed for Compressive and Tensile Loading Conditions in Lamina Emergent Mechanisms,” *Mechanism and Machine Theory*, 56, 1-15.

[8] Chen, G. and Howell, L. L., 2017, “Symmetric Equations for Evaluating Maximum Torsion Stress of Rectangular Beams in Compliant Mechanisms,” *Chinese Journal of Mechanical Engineering*, 30, submitted.

[9] Zirbel, S. A., Lang, R. J., Thomson, M. W., Sigel, D. A., Walkemeyer, P. E., Trease, B. P., Magleby, S. P., Howell, L. L., 2013, “Accommodating Thickness in Origami-Based Deployable Arrays,” *ASME Journal*

of Mechanical Design, 135, 1, 111005.

[10] Ku, J. S., 2017, “Folding thick materials using axially varying volume trimming,” *ASME 2017 International Design Engineering Technical Conferences and Computers and Information in Engineering*

Conference, Cleveland, Ohio, USA, August 6-9, 2017, DETC2017-67577.

[11] Blanding, D. L., Exact Constraint: Machine Design Using Kinematic Processing. ASME Press, 1999.

[12] Hopkins, J. B. and Culpepper, M. L., 201, “Synthesis of multi-degree of freedom, parallel flexure system concepts via freedom and constraint topology (FACT)–Part I: Principles,” *Precision Engineering*, 34, 259-270.

[13] Trease, B. P., Moon, Y.-M., and Kota, S., 2005, “Design of large-displacement compliant joints,” *ASME J. Mech. Des.*, 127(7), 788-798.

[14] Machekposhti, D. F., Tolou, N. and Herder, J. L., 2015, “A Review on Compliant Joints and Rigid-Body Constant Velocity Universal Joints Toward the Design of Compliant Homokinetic Couplings,” *ASME J. Mech. Des.*, 137(3), 032301.

[15] Haringx, J. A., 1949, “The Cross Spring Pivot as a Constructional Element,” *Appl. Sci. Res., Sect. A*, A1(5-6), pp. 313-332.

[16] Smith, S. T., 2000. *Flexures: Elements of Elastic Mechanisms*. Gordon and Breach Science, New York.

[17] Hao, G., Kong, X. and Reuben, R. L., 2011, “A nonlinear analysis of spatial compliant parallel modules: Multi-beam modules,” *Mechanism and Machine Theory*, 46(5), pp.680-706.

[18] Sen, S. and Awtar, S., 2013, “A closed-form nonlinear model for the constraint characteristics of symmetric spatial beams,” *ASME J. Mech. Des.*, 135(3), p. 031003.

[19] Hao, G., 2013, “Simplified PRBMs of spatial compliant multi-beam modules for planar motion,” *Mech. Sci.*, 4, pp. 311-318.

[20] Chen, G. and Bai, R., 2016, “Modeling large spatial deflections of slender bisymmetric beams in com pliant mechanisms using chained spatial-beam constraint model,” *ASME J. Mech. Rob.*, 8(4), p.041011.

[21] Howell, L. L., 2001, “Compliant Mechanisms,” Wiley-Interscience, New York, NY.

[22] Chen, G., Shao, X., and Huang, X., 2008, A new generalized model for elliptical arc flexure hinges,” *Rev. Sci. Instrum.*,”79(9): 095103.

[23] Chen, G, Howell, L. L., 2009, Two general solutions of torsional compliance for variable rectangular cross-section hinges in compliant mechanisms,” *Precis. Eng.*,”33: 268-274.

[24] Ma, F. and Chen, G., 2017, “Bi-BCM: A Closed-Form Solution for Fixed-Guided Beams in Compliant Mechanisms,” *ASME J. Mech. Robot.*,”9(1), 014501.

[25] Awtar, S., Slocum, A. H., and Sevincer, E., 2007, “Characteristics of Beam-Based Flexure Mod ules,” *ASME J. Mech. Des.*, **129**(6): 625-639.

[26] Homer, E.R., Harris, M.B., Zirbel, S.A., Kolodziejska, J.A., Kozachkov, H. Trease, B.P., Borgonia, J.C., Agnes, G.S., Howell, L.L., and Hofmann, D.C., 2014, “NewMethods for Developing andManufacturing Compliant Mechanisms Utilizing Bulk Metallic Glass,” *Advanced Engineering Materials*, 16(7), pp. 850- 856.

[27] Morgan, J., Magleby, S. P., Lang, R. J. and Howell, L. L., 2008, “A Preliminary Process for Origami Adapted Design,” *ASME 2015 International Design Engineering Technical Conferences and Computers and Information in Engineering Conference*, Boston, Massachusetts, USA, August 2-5, 2015, DETC2015-47559.

[28] Safsten, C. A., Fillmore, T. B., Logan, A. E., Halverson, D. M., Howell, L. L., 2016, “Analyzing the Stability Properties of Kaleidocycles,” *Journal of Applied Mechanics*, Vol. 83, No. 5, pp. 051001.

[29] Baker, J. E., 1980, “Analysis of the Bricard linkages,” *Mechanism and Machine Theory*, vol. 15, no. 4, pp. 267C286.

[30] Hanna, B.H., Lund, J.M., Lang, R.J., Magleby, S.P. and Howell, L.L., 2014, “Waterbomb base: a sym metric single-vertex bistable origami mechanism,” *Smart Materials and Structures*, 23(9), p. 094009.

[31] Bowen, L., Springsteen, K., Feldstein, H., Frecker, M., Simpson, T.W. and von Lockette, P., 2015, “Development and validation of a dynamic model of magneto-active elastomer actuation of the origami waterbomb base,” *ASME J. Mech. Robot.*,”7(1), p. 011010.

[32] Crivaro, A., Sheridan, R., Frecker, M., Simpson, T.W. and Von Lockette, P., 2016, “Bistable compli ant mechanism using magneto active elastomer actuation,” *Journal of Intelligent Material Systems and Structures*, 27(15), pp.2049-2061.

[33] Qiu, C., Zhang, K. and Dai, J.S., 2016, “Repelling-screw based force analysis of origami mechanism s,” *ASME J. Mech. Robot.*,”8(3), p. 031001.

[34] Chen, Y., Feng, H., Ma, J., Peng, R. and You, Z., 2016, “Symmetric waterbomb origami,” *Proc. R. Soc.*, A 472(2190), p. 20150846.

[35] Baker, J. E., 1980, “An Analysis of the Bricard Linkages,” *Mech. Mach. Theory*, 15(4), pp.

267-286. 20

[36] You, Z., and Chen, Y., 2001, Motion Structures, Taylor and Francis, London.

[37] Song, C. Y., Chen, Y., and Chen, I. M., 2014, “Kinematic Study of the Original and Revised General Line-Symmetric Bricard 6R Linkages,” *ASME J. Mech. Rob.*, 6(3), p. 031002.

[38] Wei, G., and Dai, J. S., 2014, “Origami-Inspired Integrated Planar-Spherical Overconstrained Mecha nisms,” *ASME J. Mech. Des.*, 136(5), p. 051003.

[39] Chen, Y., Peng, R., and You, Z., 2015, “Origami of Thick Panels,” *Science*, 349(6246), pp. 396-400.

[40] Hao, G. and Kong, X., 2013, “A normalization-based approach to the mobility analysis of spatial compliant multi-beam modules,” *Mechanism and Machine Theory*, 59, pp.1-19.